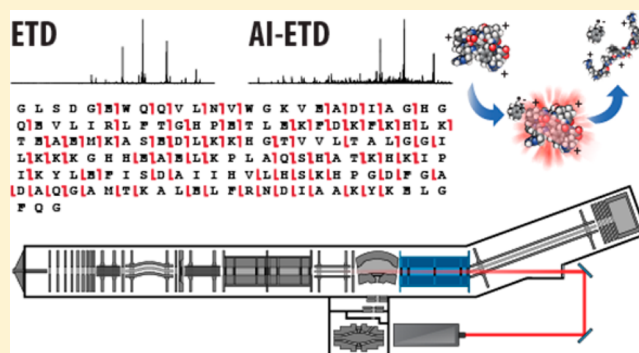


Activated Ion Electron Transfer Dissociation for Improved Fragmentation of Intact Proteins

Nicholas M. Riley,^{†,‡} Michael S. Westphall,[‡] and Joshua J. Coon^{*,†,‡,§}

[†]Department of Chemistry, [§]Department of Biomolecular Chemistry, and [‡]Genome Center of Wisconsin, University of Wisconsin, Madison, Wisconsin 53706, United States

ABSTRACT: Here we report the first implementation of activated ion electron transfer dissociation (AI-ETD) for top down protein characterization, showing that AI-ETD definitively extends the m/z range over which ETD can be effective for fragmentation of intact proteins. AI-ETD, which leverages infrared photon bombardment concurrent to the ETD reaction to mitigate nondissociative electron transfer, was performed using a novel multipurpose dissociation cell that can perform both beam-type collisional dissociation and ion–ion reactions on an ion trap–Orbitrap hybrid mass spectrometer. AI-ETD increased the number of c - and z -type product ions for all charge states over ETD alone, boosting product ion yield by nearly 4-fold for low charge density precursors. AI-ETD also outperformed HCD, generating more matching fragments for all proteins at all charge states investigated. In addition to generating more unique fragment ions, AI-ETD provided greater protein sequence coverage compared to both HCD and ETD. In all, the effectiveness of AI-ETD across the entirety of the m/z spectrum demonstrates its efficacy for robust fragmentation of intact proteins.



The advent of electron-driven dissociation mechanisms for peptide and protein characterization via mass spectrometry (MS) has sustained more than 15 years of innovation in proteomics. Electron capture dissociation (ECD)¹ and electron transfer dissociation (ETD)² have especially enabled advances in top down proteomics, in which intact proteins rather than peptide surrogates are interrogated for sequence information.^{3–5} Building on developments afforded by ECD and ETD, the top down approach has recently gained popularity due to its potential for complete protein characterization, including information about genetic variants, alternative splicing, and combinatorial patterns of post-translational modifications (PTMs).^{6,7} In intact protein analysis, traditional slow-heating methods, such as collision-activated dissociation (CAD) and infrared multiple photon dissociation (IRMPD), cleave selectively at the most labile bonds, limiting both the extent of fragmentation achievable and the ability to localize PTMs.^{8,9} Alternatively, ECD and ETD facilitate fragmentation of peptide and protein backbone bonds while retaining PTMs, providing more extensive and informative cleavage of proteins than CAD and IRMPD.^{4,5,10,11} Other fragmentation schemes, such as surface-induced dissociation (SID)¹² and ultraviolet photo-dissociation (UVPD),¹³ have also demonstrated utility as nontraditional dissociation methods for top down proteomics, although ECD and ETD remain the most widely used alternative to collision-based methods for protein characterization.^{14–16}

Even with their prevalence in top down analyses, ECD and ETD have limitations that require consideration. One of the

most formidable barriers for practitioners of these techniques is a strong dependence on precursor charge density, greatly limiting their effectiveness as precursor mass-to-charge (m/z) values increase. In a process called nondissociative electron capture/transfer (ECnoD/ETnoD), backbone cleavage often occurs, but no sequence information is provided because the product ions are held together by noncovalent interactions, which become more pronounced at lower precursor charge densities.^{17–20} To combat ECnoD and ETnoD and, accordingly, improve generation of sequence-informative product ions, additional energetic activation can be supplied to disrupt the secondary gas-phase structure associated with lower charge densities.²¹ Collectively described as “activated ion” ECD (AI-ECD), several methods have emerged for introducing this additional energy before, during, and after the ECD reaction using collisions,²² infrared (IR) photons,^{22–24} raised ambient temperature,^{17,25} and collisions with high energy electrons;²⁶ these methods have shown tremendous success in increasing ECD product ion yield for protein cations and have extended the utility of ECD for top down applications.

Supplemental activation with ETD, however, is more challenging and has only been extensively studied at the peptide level.^{27–30} Higher pressures in ETD reaction cells (approximately 10^6 times higher than ICR cells where ECD is performed) not only make ETD more susceptible to ETnoD,

Received: March 5, 2015

Accepted: June 11, 2015

Published: June 11, 2015

but also cause more pronounced collisional cooling of precursor cations, making collisional pre-activation of precursor ions largely ineffective.^{31,32} Postreaction activation of ETnoD products with gentle collisions (termed ETcaD) produces more extensive and intense fragment ions from N- α backbone cleavages for peptide cations, but many fragments generated have skewed isotope distributions due to hydrogen abstractions.^{29,33,34} Ideally then, activation would be applied concurrently with the ETD reaction; collisional activation of the precursor ions, however, requires resonant excitation during ETD, increasing the velocity of the ions and inhibiting ion-ion reactions.³⁵⁻³⁷ Instead, we have introduced a viable alternative, IR photon (10.6 μm) irradiation concurrent to the ETD reaction, termed activated ion ETD (AI-ETD), and have shown the benefits it affords peptide fragmentation for shotgun analyses.^{30,38,39}

Despite the success of AI-ETD in peptide fragmentation and the enhancements seen with AI-ECD for intact protein analysis, AI-ETD has yet to be widely applied to top down proteomics. Where ECD and AI-ECD are largely limited to FT-ICR instruments, AI-ETD can be implemented on virtually any instrument that has an rf trapping device, making it an appealing tool for ubiquitous use in the top down field. Indeed, enhancing ETD reactions for intact protein characterization is currently an active field, reflecting the demand for the development of AI-ETD methods. Costello and co-workers recently highlighted the effects of pre- and postactivation with collisions and IR photons on ETD reactions (preAI-ETD and postAI-ETD) of a single glycoprotein (RNaseB) and its nonglycosylated analog (RNaseA), surprisingly showing enhanced fragmentation with preactivation for ETD conducted in a hexapole on an ICR instrument.⁴⁰ Additionally, Brodbelt and co-workers demonstrated the benefits of combining UVPD and ETD just last year, producing *a*-, *b*-, *c*-, *x*-, *y*-, and *z*-type fragment ions for extensive fragmentation of intact proteins.⁴¹ Most recently yet, the Heck group published the benefits higher energy collisional dissociation of ETD products (ETHcD) can have in extending sequence coverage and localizing modification sites.⁴²

We have recently developed a multipurpose dissociation cell (MDC) specifically for ion-ion reactions for top down applications.⁴³ The MDC enables both HCD and improved ETD fragmentation, allowing faster ETD reaction times and larger precursor ion populations for improved fragment ion signal-to-noise. The placement of MDC is ideal for implementing AI-ETD on a hybrid ion trap-Orbitrap mass spectrometer because a continuous wave CO₂ laser can be easily introduced concentrically to the trapping volume of the MDC.³⁹ Here we report the first implementation of AI-ETD (i.e., concurrent irradiation with IR photons) for intact protein analysis of five protein standards with molecular weights ranging from ~8.6 to 29 kDa. Using the MDC as the sole reaction cell, we compare fragment ion production with HCD, ETD, and AI-ETD, demonstrating the considerable improvement AI-ETD can offer over ETD and HCD for product ion generation and overall protein sequence coverage. This work showcases the clear advantage AI-ETD has to produce robust fragmentation across a broad range of precursor charge densities for a variety of proteins, giving it compelling potential for top down proteomics, especially for high-throughput experiments.

MATERIALS AND METHODS

Mass Spectrometry Instrumentation. The multipurpose dissociation cell (MDC) and affixed laser have been described previously.^{39,43} Briefly, the MDC replaces the pre-existing HCD cell in the hybrid ion trap-Orbitrap Elite system,⁴⁴ retaining its basic geometry, but requiring additional electronics to supply higher trapping rf voltages, axial rf voltages for charge-sign independent trapping, and independently controlled DC biases to its four sections. Cation precursors were sequestered in the front sections, and reagent anions were accumulated in the back sections. For the ETD reaction, all DC voltages of the MDC were set to 0 V, and the axial confining rf was applied. The reaction was quenched by setting the center sections to a negative DC offset, and product ions were transferred to the C-trap using an identical extraction gradient used for HCD scans. AI-ETD was performed by irradiating the trapping volume of the MDC during the entirety of the ETD reaction with a Firestar T-100 Synrad 100-W CO₂ continuous wave laser (Mukilteo, WA). The laser was introduced into the cell via an excavated ion passage in the reagent ion transfer multipole and a ZnSe window that was installed concentric to the MDC. Using instrument firmware and modification to instrument code in conjunction with a gated laser controller, laser power output (in Watts) from a continuous wave CO₂ laser (10.6 μm) was modulated remotely through voltage inputs to the controller and was triggered to fire only during the ETD reaction as it was being conducted in the MDC. Laser power was adjusted and is reported as a percentage of total output (100 W). See the abstract graphic for an instrument diagram.

Materials, Reagents, and Sample Preparation. All protein standards (ubiquitin [B4DV12], cytochrome C [P00004], α -lactalbumin [P00711], myoglobin [P68082], and carbonic anhydrase [P00921]) were purchased as mass spectrometry grade standards from Protea Biosciences (Morgantown, WV). Formic acid ampules and acetonitrile were purchased from Thermo Scientific (Rockford, IL), and an infusion syringe was purchased from Hamilton (Reno, NV). All protein standards were resuspended at approximately 10 picomole per microliter in 49.9:49.9:0.2 acetonitrile/water/formic acid. Because of known disulfide bonds, α -lactalbumin was reduced and alkylated before being resuspended for infusion. Here, the lyophilized protein standard was resuspended in 8 M urea, 50 mM Tris, pH 8, and free cysteines were reduced with 15 mM dithiothreitol (DTT) for 45 min at 58 °C and alkylated with 45 mM iodoacetamide (IAA) for 45 min in the dark at room temperature. Alkylation was stopped by the addition of 5 mM DTT. The sample was then desalted using a C2 SepPak (Waters).

ESI-MS/MS Analysis. Proteins were infused via syringe pump into the mass spectrometer at 5 $\mu\text{L}/\text{min}$ through a 500 μL syringe and were ionized with electrospray ionization (ESI). Full MS spectra were collected at a resolution of 240000 at 400 *m/z* with 3-5 microscans and a target AGC of 3e6 ions. All MS/MS scans were performed in the Orbitrap, also at a resolution of 240000 at 400 *m/z*, with a target AGC of 3e5 to 8e5 ions and isolation widths of 3-5 *m/z*. Each MS/MS scan was collected using 3 microscans and 3 precursor injections (i.e., "fills") per scan.⁴³ For all ETD and AI-ETD experiments, the nitrogen pressure in the MDC was lowered to a ΔN_2 pressure of $\sim 0.1 \times 10^{-10}$ Torr, as measured by the Penning gauge in the Orbitrap chamber, to prevent collisional cooling that negates the additional energy supplied by the infrared laser.

Gas pressure was left at normal operating levels for HCD scans to ensure proper collisional dissociation (ΔN_2 of $\sim 0.3 \times 10^{-10}$ Torr); although this may introduce bias between ETD and HCD data, we felt it was the best compromise to achieve sufficient HCD fragmentation on our system and saw no detriment from the slightly higher pressure on HCD spectra of myoglobin when testing the pressure settings. A fixed accumulation time of 5 ms was used for fluoranthene reagent anions (m/z 202) for ETD and AI-ETD experiments and reactions time varied from 3.5 to 10 ms. Laser power output ranged from 50 to 80% and HCD collision energies ranged from 12 to 25 nCE. All dissociation events occurred in the MDC.

Data Analysis. MS/MS RAW files were converted to mzXML format with MSConvert, followed by spectral deconvolution with MS-Deconv.^{45,46} Maximum mass was set to the protein mass plus 1000 Da, maximum charge was set to the precursor charge state, the m/z tolerance was set to 0.02, and the signal-to-noise ratio was set to 2. ProSight Lite was used to generate matched fragments from decharged and deisotoped peak lists for each protein.⁴⁷ Protein sequences were loaded individually into ProSight Lite, and peak lists from individual scans were matched against theoretical peaks within a 10 ppm tolerance. HCD data was matched against b/y ions, and c/z ions were matched against for ETD and AI-ETD. Known signal peptides/pro-peptide sequences and N-terminal methionines were removed from the protein sequences (except ubiquitin) before matching with ProSight Lite, and modifications were incorporated into the sequence used for matching based on known modifications in UniProt. Proteins were matched with the following modifications: myoglobin and ubiquitin: none; cytochrome C: N-terminal acetylation (+42.01 Da) and a heme C group mass shift (+615.17 Da) on cysteine 15; α -lactalbumin: fixed carbamidomethylation of cysteines (+57.01 Da); carbonic anhydrase: N-terminal acetylation (+42.01 Da).

RESULTS AND DISCUSSION

AI-ETD Improves Fragmentation across Charge State Envelopes. Nondissociative electron transfer becomes increasingly prevalent as precursor charge density decreases, causing precursor-to-product ion conversion in ETD reactions to deteriorate at higher m/z values. We have shown previously that disrupting secondary gas phase structure with concurrent IR photo-activation can increase ETD product ion yield for peptide cations, converting ETnoD products into c- and z-type fragment ions. We hypothesized that AI-ETD could similarly benefit dissociation of protein cations by aiding in protein unfolding in the gas phase during the ETD reaction to promote sequence-informative product ion formation over ETnoD, especially for precursors with m/z values greater than 1000 Th. To first test this hypothesis, we benchmarked ETD fragment ion production for 12 charge states ($z = 8-19$) of cytochrome C (~ 12.3 kDa), with precursor m/z values spanning $\sim 650-1550$ Th. To display the abundance of each precursor, the charge state envelope is shown in gray in Figure 1 (top panel). ETD performance was evaluated by measuring the production of *unique* matching fragments for each charge state. Note, here and throughout, the term unique fragments indicates only the number of distinct c- and z-type ions observed, disregarding the number of matches a fragment may have had at different charge states. Thus, the number of *total* matching fragments encompasses all instances of c- and z-type fragments detected,

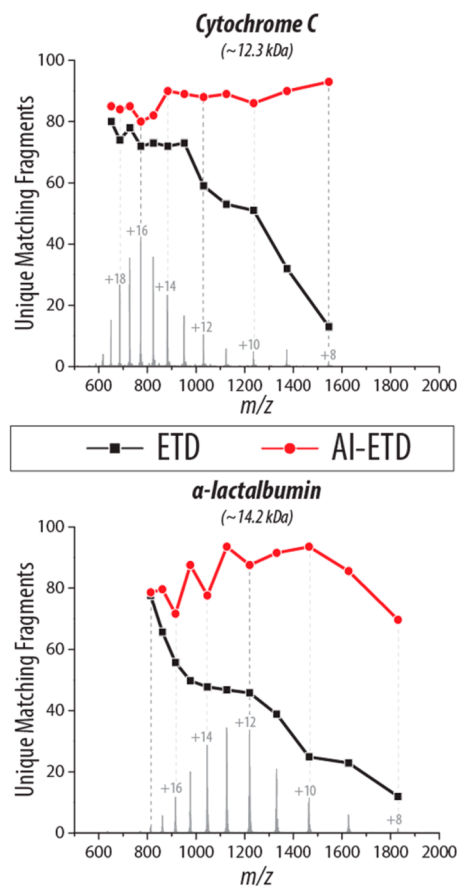


Figure 1. AI-ETD maintains robust protein fragmentation across the charge state envelope. Cytochrome C (top) and α -lactalbumin (bottom) are roughly the same molecular weight, yet they give appreciably different charge state distributions (gray background insets). The ETD product ion yield drops as precursor m/z values increase, while AI-ETD sustains a high level of c- and z-type product ion formation at all m/z values (black and red traces, respectively) for dissociation of either protein.

including multiple counts of the same fragment if detected at more than one charge state. ETD performed well for the majority of the charge states of cytochrome C, producing 80 unique fragments for the most charge dense precursor investigated ($z = +19$) and never generating fewer than 72 unique fragments for charge states $z \geq +13$. The number of fragments produced significantly decreased, however, once precursor m/z values exceeded 1000 Th, falling to just 13 unique fragments at $z = +8$, which represents a greater than 6-fold depreciation in fragment ion production. The same set of precursors were then fragmented with AI-ETD, which outperformed ETD in all cases and improved product ion generation by more than 7-fold for the lowest charge density precursors (Figure 1, top panel). In fact, AI-ETD produced at least 80 unique fragments for every precursor across the entire charge state distribution.

To confirm these results, we compared ETD and AI-ETD for a protein that is similar in size but displays a considerably different charge state distribution; the bottom panel of Figure 1 presents the same evaluation of ETD and AI-ETD described above with α -lactalbumin (~ 14.2 kDa). Despite similarities in molecular weight to cytochrome C, α -lactalbumin has a charge state distribution that favors less charge dense precursors, with the most intense charge states ($+11 \leq z \leq +14$) falling in the

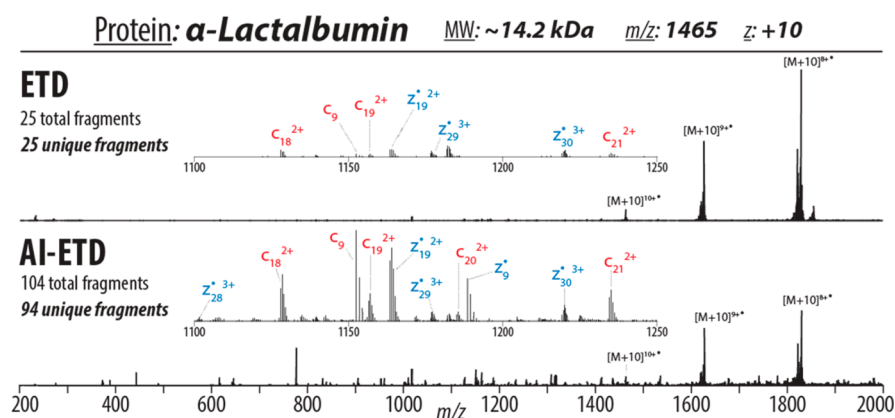


Figure 2. Comparison of ETD and AI-ETD MS/MS. Each tandem mass spectrum, from a single scan representing three averaged transients, was generated following ETD (top) or AI-ETD (bottom) of the +10 charge state of α -lactalbumin. Note both spectra are on the same intensity scale. Insets, also shown on the same intensity scale, show annotated peaks from each spectrum for the given m/z range.

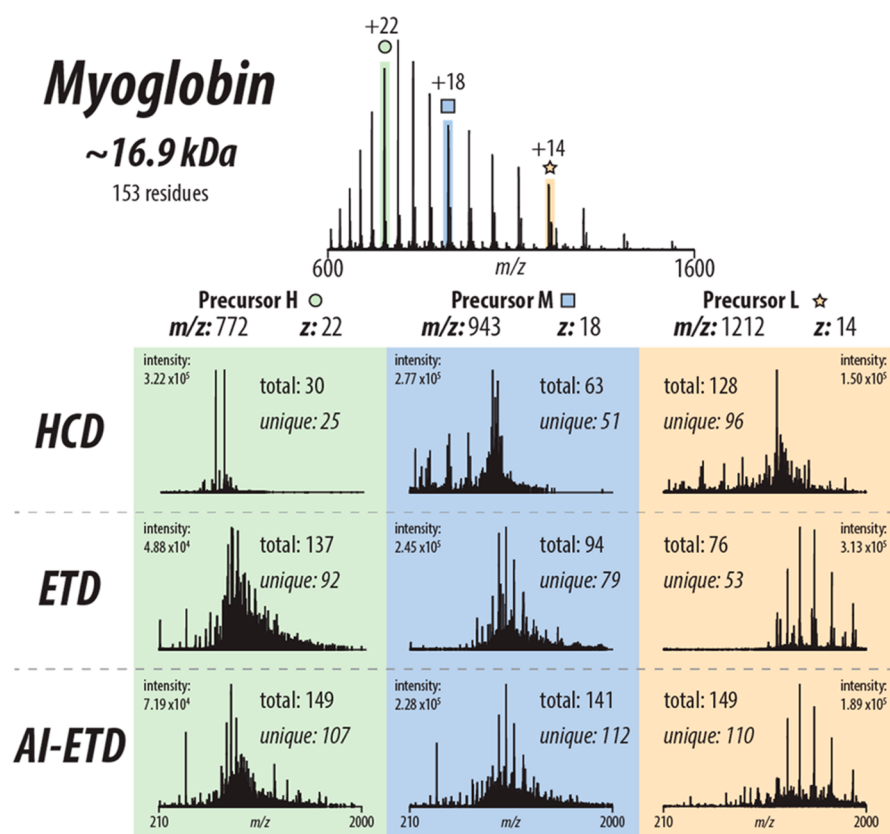


Figure 3. Comparison of HCD, ETD, and AI-ETD for dissociation of myoglobin precursors having high, moderate, and low charge densities. Three precursors of myoglobin were selected for MS/MS fragmentation with HCD, ETD, and AI-ETD, as indicated in the MS spectrum by respective symbols and color. Precursor H is the most charge dense while Precursor L is the least. Each spectrum results from a single scan (representing three averaged transients).

1000–1400 Th region. Figure 1 (bottom panel) shows the charge state envelope for α -lactalbumin in gray. Here, ETD fragment ion production steadily declines from 78 unique fragments for the most charge dense precursor ($m/z \sim 814$ Th, $z = +18$) to 12 unique fragments for the precursor with the lowest charge density ($m/z \sim 1831$ Th, $z = +8$). Unlike cytochrome C, the most abundant charge states for α -lactalbumin, and thus, the most likely charge states to be selected in top down experiments would be outside the ideal m/z range for ETD fragmentation, yielding suboptimal sequence characterization due to ETNoD. As with cytochrome

C, however, AI-ETD outperforms ETD for all charge states of α -lactalbumin, maintaining optimal fragment ion production for all precursors. The numbers of unique matching fragments drop off slightly for the highest m/z values of α -lactalbumin, although AI-ETD still provides ~ 3.75 - to 5.8-fold increases in product ion yield over ETD for the lowest charge states.

To provide an example of spectral quality we present Figure 2, which shows a comparison of spectra from ETD and AI-ETD for the +10 charge state of α -lactalbumin ($m/z = 1465$). These data provide a visual confirmation of the boosts in product ion generation AI-ETD provides. The increase in number and

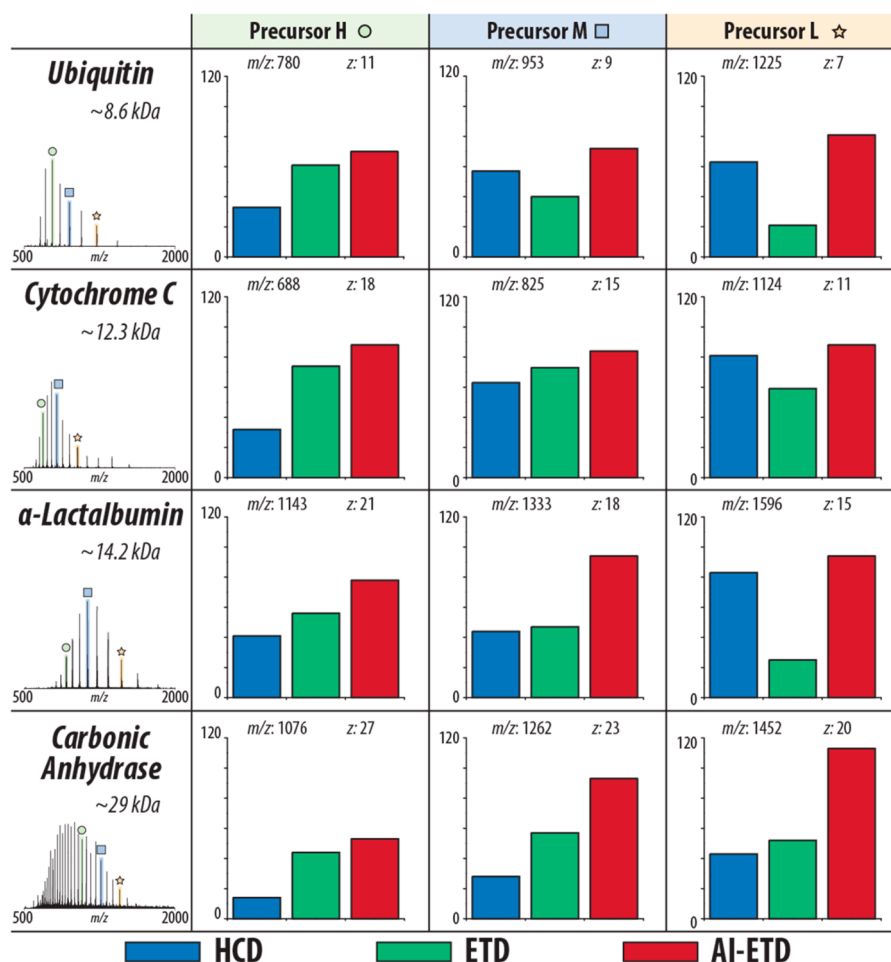


Figure 4. AI-ETD, HCD, and ETD performance for several proteins. Each bar graph represents the number of unique matching fragments detected following with HCD, ETD, and AI-ETD-MS/MS. Each precursor selected is indicated in its respective MS¹ spectrum by symbol and color, and precursor charge and approximate *m/z* value are indicated for each condition. Precursor charge density decreases from Precursor H to Precursor L for each protein. Matching fragments were determined from single scans for each condition.

intensity of product ions, highlighted by the annotated inset, is matched with a decrease in ETnoD products, which is easily discernible as the two spectra and corresponding insets are on the same respective intensity scales. The additional energy provided by IR photons interrupts noncovalent interactions of the protein precursor ions, promoting a greater conversion of precursor ions to *c*- and *z*-type product ions. This example is especially representative of low charge density precursors for all proteins investigated in this study, where ETD produces relatively few product ions while AI-ETD provides abundant fragmentation.

Interesting to note, the extensive ETD fragmentation achieved even with low charge density precursors indicates that precursor protein ions are not being completely unfolded by IR photoactivation into linear molecules where charged residues would be remote from many backbone bonds along the protein sequence; rather, we believe the concurrent heating by IR photons disrupts noncovalent interactions to unfold precursors into an intermediate state that still has nonlinear conformation, which is supported by previous work from McLafferty and co-workers.⁴⁸ Thus, rather than activated precursors being completely denatured into linear molecules in AI-ETD, these partially unfolded intermediate conformations still keep regions of the protein backbone in close enough proximity to charged residues to promote cleavage per the

accepted ETD mechanism, even though they may not be directly adjacent (in sequence) to a charged residue. Clearly, this point-of-view can be further examined by experiments outside of the scope of this work, including hydrogen–deuterium exchange and ion mobility experiments.

Comparison of HCD, ETD, and AI-ETD for Five Protein Standards. We extended our study of AI-ETD to other protein standards to explore the viability of AI-ETD for proteins across a broader molecular weight range. In addition to cytochrome C and α -lactalbumin, we selected ubiquitin (~8.6 kDa), myoglobin (~16.9 kDa), and carbonic anhydrase (~29 kDa). For each of these proteins, we chose three precursors representing relatively high charge density (Precursor H), moderate charge density (Precursor M), and low charge density (Precursor L) and dissociated each with HCD, ETD, and AI-ETD.

To compare the performance of the three dissociation methods we focused first on myoglobin (Figure 3). Expected trends for precursor charge state dependence arose for both HCD^{49,50} and ETD when assessing performance for all three peaks selected; HCD functioned its best for the lowest charge density precursor, producing 96 unique fragments for Precursor L (but only 25 fragments for Precursor H), while ETD performed most favorably for the highest charge density precursor, generating 92 unique fragments for Precursor H (but

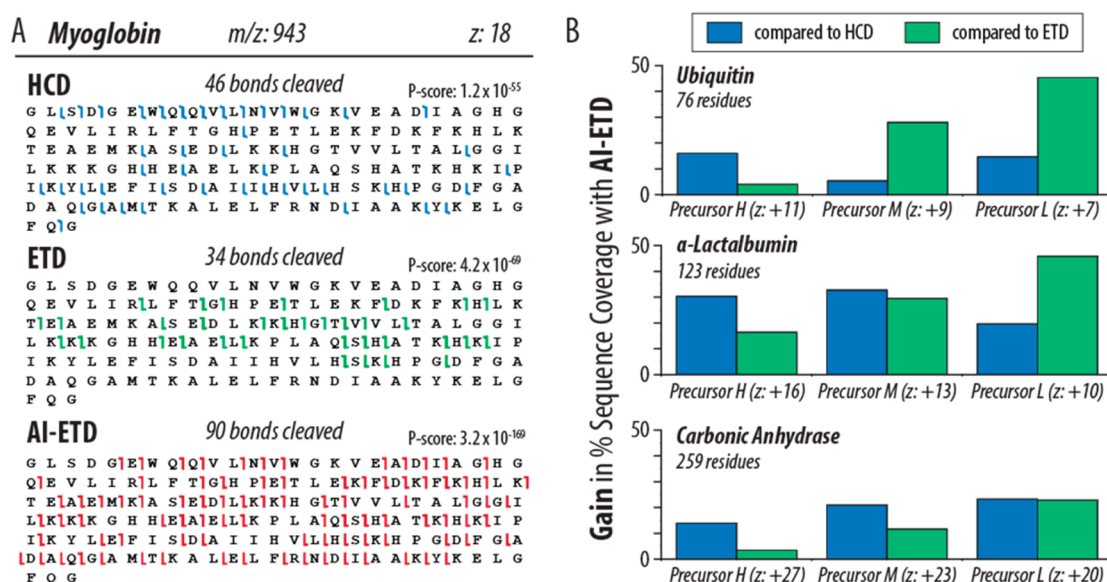


Figure 5. AI-ETD increases protein sequence coverage compared to ETD and HCD. (A) Sequence coverage maps of myoglobin show bonds cleaved in a single scan by HCD, ETD, and AI-ETD for the +18 charge state. Number of total bonds cleaved and calculated P-score from ProSight Lite are provided. (B) The gains in sequence coverage offered by AI-ETD in comparison to HCD and ETD are shown for three proteins spanning the molecular weight range studied in this experiment. Data shown for each protein correspond to the precursors shown in Figure 4. AI-ETD increases protein sequence coverage in all cases shown here.

only 53 fragments for Precursor L). Contrary to this, AI-ETD performed consistently well for all three precursors selected. AI-ETD generates 15 more unique fragments and 12 more total fragments than ETD for Precursor H and maintains robust fragmentation for Precursor M (112 unique and 141 total), despite the significant decrease seen with ETD alone. The ability of AI-ETD to effectively negate the charge density dependence seen with ETD is even more evident for Precursor L, where AI-ETD more than doubles the number of unique fragment ions (110 vs 53) and nearly doubles the number of total fragments produced with ETD (149 vs 76). AI-ETD also provides similar gains in fragment ion production over HCD, producing the highest number of both unique and total fragments for all three precursors.

Trends in base peak intensity for the three fragmentation methods also arise (Figure 3). The steady decrease in base peak intensity for HCD across Precursor H to Precursor L illustrates the shift from a handful of intense fragment ions dominating the spectra to a greater number of fragment ions accounting for larger spread in the distribution of total ion current (TIC). Conversely, the base peak intensities for ETD spectra increase from Precursor H to Precursor L, mainly because charge reduced species, which consist of ETnoD products, become more intense relative to the product ion signal. Charge reduced species comprise only 4.79% of the TIC for the ETD spectrum of Precursor H, indicating a relatively efficient conversion of precursor to fragments. This proportion increases to 8.89% of the TIC for Precursor M, reflecting the decrease in fragment ion generation due to the lower precursor charge density. The greatest extent of ETnoD is observed following ETD dissociation of Precursor L: 21.8% of the TIC is represented by charge reduced species. With AI-ETD, however, charge reduced species account for only 5.96, 7.31, and 11.4% of the TIC for Precursors H, M, and L, respectively, indicating that AI-ETD maintains its robust generation of c- and z-type ions by converting ETnoD products produced with ETD to

sequence informative product ions for lower charge density precursors like Precursor M, and especially Precursor L.

Next we extended this experiment to a broader set of proteins. Figure 4 summarizes the results of HCD, ETD, and AI-ETD for these experiments for the other four protein standards. Again, the expected proclivity for low charge density precursors with HCD and high charge density precursors with ETD is observed: HCD produces more fragment matches for higher m/z Precursor L for each protein, whereas ETD performs the best on Precursor H and declines in fragment ion production as m/z values increase. A noticeable exception occurs for carbonic anhydrase, where ETD generates slightly more products for the lowest charge state. We surmise this discrepancy occurs not because of the improved performance of ETD for this precursor but rather from challenges that arise with spectral deconvolution of MS/MS spectra of relatively large proteins with few transients averaged. ETD of highly charged precursors of large proteins, such as Precursor H of carbonic anhydrase, generates many highly charged product ions that can occur in a relatively narrow m/z range. This, coupled with low product ion signal-to-noise, presents challenges with delineating the proper isotope distributions, and thus charge states, of product ions.^{51,52} Often signal-to-noise is improved by increasing the number of transients averaged, especially for larger proteins. For example, if averaging 10 scans (30 total transients) instead of one scan (3 total transients), the number of fragments seen for ETD of Precursor H increases from 44 to 81 unique fragments. We elected here to keep a consistent use of one scan (three averaged transients) for all proteins, including carbonic anhydrase, to maintain short overall acquisition times. Additionally, with high charge states, like Precursor H especially, over-reaction due to longer than desired ETD reaction times can cause degradation of primary fragment ions, yielding fewer sequence informative products. This may have played a role in these analyses, considering the faster reaction times afforded by the higher RF fields in the MDC, which make very fast

reactions more challenging to control. We do also note that the slightly higher pressures in the MDC for HCD may have had more of a pronounced effect here with carbonic anhydrase, the largest of the proteins analyzed, although the trends seen are consistent with other published data.^{13,44}

As with myoglobin, AI-ETD both outperforms HCD and ETD for every precursor analyzed, and also produces relatively constant numbers of fragment ions for all precursors of a given protein (Figure 4). These results demonstrate that AI-ETD offers favorable fragmentation of intact proteins with molecular weights in the range typically explored in high-throughput proteomics (<30 kDa) for precursors with highly variable charge densities. In typical top down experiments, precursors selected for MS/MS scans vary greatly in their charge density, prompting many researchers to conduct back-to-back HCD and ETD scans on the same peak.^{53,54} This doubles the amount of time needed to investigate each precursor and, thus, limits throughput. Recent work has shown how precursors can be judiciously chosen based on m/z and charge,⁵⁵ but this is not straightforward to implement. Because AI-ETD extensively fragments precursors at diverse charge states across the m/z range, we conclude that AI-ETD may prove useful as a sole fragmentation method, eliminating the need to selectively choose “ideal” charge states of precursors for a given fragmentation method. Moreover, this would effectively halve the cycle time needed per precursor, increasing the throughput achievable in a given experiment, while still offering the best possible dissociation.

Benefits of AI-ETD for Protein Sequence Coverage.

Beyond generating more fragments than HCD and ETD, AI-ETD also translates to greater protein sequence coverage (the number of bonds cleaved divided by the total number of bonds). High protein sequence coverage is paramount to realizing the potential of top down proteomics, but maximal sequence coverage must often be compromised for the speed needed for high-throughput experiments; the coupling of fragmentation methods in back-to-back scans can offer greater protein characterization but the costs incurred in instrument duty cycle ultimately limit the dynamic range achievable in a given experiment.^{53–56} Innovations in fragmentation methods are making greater protein sequence coverage for high-throughput experiments more attainable,⁵⁷ and AI-ETD represents a significant step forward in sequence coverage achievable per scan over current methods. Figure 5A shows a sequence map for the bonds cleaved in a single scan with each of the three fragmentation methods for the +18 charge state of myoglobin. AI-ETD offers a nearly 2-fold increase in the number of bonds cleaved over HCD (90 vs 46) and a 3.65-fold increase over ETD (90 vs 34). Greater numbers of unique fragments generated by AI-ETD not only translate to more bonds cleaved, but also increase the confidence of the protein identification, indicated by the P-score for each (from ProSight Lite). Figure 5B demonstrates the gains in percent sequence coverage seen with AI-ETD over both HCD and ETD for three precursors fragmented for ubiquitin, α -lactalbumin, and carbonic anhydrase (corresponding to the experiments described above). These three proteins span the molecular weight range of a typical top down experiment, underscoring the improvement in sequence coverage AI-ETD can offer over HCD and ETD for all proteins in a complex sample, regardless of protein size or precursor charge.

CONCLUSIONS

We have demonstrated the first implementation of concurrent IR photoactivation during ETD, that is, AI-ETD, for improved fragmentation of intact proteins. Using a multipurpose dissociation cell modified to conduct both ion–ion reactions and collisional dissociation, we have shown the significant improvement of sequence-informative fragment ion production AI-ETD can offer for low charge density precursors, which usually yield poor fragmentation with ETD alone. Furthermore, we illustrated that AI-ETD consistently provides favorable product ion generation over HCD and ETD for precursors at various charge states for five protein standards spanning ~8.6 to 29 kDa.

These exciting results render AI-ETD as a new intact protein fragmentation method with high utility. Because it (1) tempers the charge state dependency that limits typical ETD fragmentation, (2) matches or improves upon the number of unique fragment ions produced by ETD in all cases investigated here, (3) matches or improves upon the number of unique fragment ions produced by the complementary collision-based HCD fragmentation method, and (4) improves protein sequence coverage, AI-ETD is well-situated as a singular fragmentation method with the flexibility to investigate a wide range of intact proteins and has the potential to be ideal for the diverse array of proteins seen in complex mixtures. Further, the elevation in product ion generation translates to considerable gains in protein sequence coverage per scan with AI-ETD. Experiments are being conducted currently to translate the advantages AI-ETD can offer top down proteomics using front end separations.⁵⁸ Moreover, the increases in fragment matches become more pronounced for larger molecular weight proteins (where more noncovalent interactions can challenge ETD fragmentation even further), indicating that AI-ETD may have utility for proteins beyond molecular weight range investigated herein, as seen with previous AI-ECD experiments.^{10,21–26} We conclude that AI-ETD is well-positioned to further the goals of complete protein characterization, a central tenet of modern top down experiments.

AUTHOR INFORMATION

Corresponding Author

*E-mail: jcoon@chem.wisc.edu.

Notes

The authors declare no competing financial interest.

ACKNOWLEDGMENTS

We thank Jae Schwartz and John Syka for helpful discussions and technical assistance. This work was supported by NIH RO1 GM080148 (J.J.C.). N.M.R. gratefully acknowledges support of an NSF graduate fellowship (DGE-1256259).

REFERENCES

- (1) Zubarev, R.; Kelleher, N. L.; McLafferty, F. W. *J. Am. Chem. Soc.* **1998**, *120*, 3265–3266.
- (2) Syka, J. E. P.; Coon, J. J.; Schroeder, M. J.; Shabanowitz, J.; Hunt, D. F. *Proc. Natl. Acad. Sci. U.S.A.* **2004**, *101*, 9528–9533.
- (3) Coon, J. J.; Syka, J. E. P.; Shabanowitz, J.; Hunt, D. *Biotechniques* **2005**, *38*, 519.
- (4) Garcia, B. A. *J. Am. Soc. Mass Spectrom.* **2010**, *21*, 193–202.
- (5) Zubarev, R. A. *Curr. Opin. Biotechnol.* **2004**, *15*, 12–16.
- (6) Catherman, A. D.; Skinner, O. S.; Kelleher, N. L. *Biochem. Biophys. Res. Commun.* **2014**, *445*, 683–693.
- (7) Smith, L. M.; Kelleher, N. L. *Nat. Methods* **2013**, *10*, 186–187.

- (8) Little, D. P.; Speir, J. P.; Senko, M. W.; O'Connor, P. B.; McLafferty, F. W. *Anal. Chem.* **1994**, *66*, 2809–2815.
- (9) Raspopov, S. A.; El-Faramawy, A.; Thomson, B. A.; Siu, K. W. M. *Anal. Chem.* **2006**, *78*, 4572–4577.
- (10) Ge, Y.; Lawhorn, B. G.; ElNaggar, M.; Strauss, E.; Park, J.-H.; Begley, T. P.; McLafferty, F. W. *J. Am. Chem. Soc.* **2002**, *124*, 672–678.
- (11) Zubarev, R. A.; Horn, D. M.; Fridriksson, E. K.; Kelleher, N. L.; Kruger, N. A.; Lewis, M. A.; Carpenter, B. K.; McLafferty, F. W. *Anal. Chem.* **2000**, *72*, 563–573.
- (12) Zhou, M.; Wysocki, V. H. *Acc. Chem. Res.* **2014**, *47*, 1010–1018.
- (13) Shaw, J. B.; Li, W.; Holden, D. D.; Zhang, Y.; Griep-Raming, J.; Fellers, R. T.; Early, B. P.; Thomas, P. M.; Kelleher, N. L.; Brodbelt, J. S. *J. Am. Chem. Soc.* **2013**, *135*, 12646–12651.
- (14) Chait, B. T. *Science* **2006**, *314*, 65–66.
- (15) Siuti, N.; Kelleher, N. L. *Nat. Methods* **2007**, *4*, 817–821.
- (16) Coon, J. J. *Anal. Chem.* **2009**, *81*, 3208–3215.
- (17) Breuker, K.; Oh, H.; Horn, D. M.; Cerda, B. A.; McLafferty, F. W. *J. Am. Chem. Soc.* **2002**, *124*, 6407–6420.
- (18) Valentine, S. J.; Counterman, A. E.; Clemmer, D. E. *J. Am. Soc. Mass Spectrom.* **1997**, *8*, 954–961.
- (19) Shelimov, K. B.; Clemmer, D. E.; Hudgins, R. R.; Jarrold, M. F. *J. Am. Chem. Soc.* **1997**, *119*, 2240–2248.
- (20) Good, D. M.; Wirtala, M.; McAlister, G. C.; Coon, J. J. *Mol. Cell. Proteomics* **2007**, *6*, 1942–1951.
- (21) Oh, H.; McLafferty, F. W. *Bull. Korean Chem. Soc.* **2006**, 389–394.
- (22) Horn, D. M.; Ge, Y.; McLafferty, F. W. *Anal. Chem.* **2000**, *72*, 4778–4784.
- (23) Mikhailov, V. A.; Cooper, H. J. *J. Am. Soc. Mass Spectrom.* **2009**, *20*, 763–771.
- (24) Tsybin, Y. O.; Witt, M.; Baykut, G.; Kjeldsen, F.; Håkansson, P. *Rapid Commun. Mass Spectrom.* **2003**, *17*, 1759–1768.
- (25) Horn, D. M.; Breuker, K.; Frank, A. J.; McLafferty, F. W. *J. Am. Chem. Soc.* **2001**, *123*, 9792–9799.
- (26) Sze, S. K.; Ge, Y.; McLafferty, F. W. *Anal. Chem.* **2003**, *75*, 1599–1603.
- (27) Xia, Y.; Han, H.; McLuckey, S. A. *Anal. Chem.* **2008**, *80*, 1111–1117.
- (28) Pitteri, S. J.; Chrisman, P. A.; McLuckey, S. A. *Anal. Chem.* **2005**, *77*, 5662–5669.
- (29) Swaney, D. L.; McAlister, G. C.; Wirtala, M.; Schwartz, J. C.; Syka, J. E. P.; Coon, J. J. *Anal. Chem.* **2007**, *79*, 477–485.
- (30) Ledvina, A. R.; McAlister, G. C.; Gardner, M. W.; Smith, S. I.; Madsen, J. A.; Schwartz, J. C.; Stafford, G. C.; Syka, J. E. P.; Brodbelt, J. S.; Coon, J. J. *Angew. Chem., Int. Ed.* **2009**, *48*, 8526–8528.
- (31) Badman, E. R.; Hoaglund-Hyzer, C. S.; Clemmer, D. E. *J. Am. Soc. Mass Spectrom.* **2002**, *13*, 719–723.
- (32) Ben Hamidane, H.; Chiappe, D.; Hartmer, R.; Vorobyev, A.; Moniatte, M.; Tsybin, Y. O. *J. Am. Soc. Mass Spectrom.* **2009**, *20*, 567–575.
- (33) O'Connor, P. B.; Lin, C.; Cournoyer, J. J.; Pittman, J. L.; Belyayev, M.; Budnik, B. A. *J. Am. Soc. Mass Spectrom.* **2006**, *17*, 576–585.
- (34) Sun, R.-X.; Dong, M.-Q.; Song, C.-Q.; Chi, H.; Yang, B.; Xiu, L.-Y.; Tao, L.; Jing, Z.-Y.; Liu, C.; Wang, L.-H.; Fu, Y.; He, S.-M. *J. Proteome Res.* **2010**, *9*, 6354–6367.
- (35) McLuckey, S. A.; Reid, G. E.; Wells, J. M. *Anal. Chem.* **2002**, *74*, 336–346.
- (36) Reid, G. E.; Shang, H.; Hogan, J. M.; Lee, G. U.; McLuckey, S. A. *J. Am. Chem. Soc.* **2002**, *124*, 7353–7362.
- (37) Chrisman, P. A.; Pitteri, S. J.; McLuckey, S. A. *Anal. Chem.* **2006**, *78*, 310–316.
- (38) Ledvina, A. R.; Beauchene, N. A.; McAlister, G. C.; Syka, J. E. P.; Schwartz, J. C.; Griep-Raming, J.; Westphall, M. S.; Coon, J. J. *Anal. Chem.* **2010**, *82*, 10068–10074.
- (39) Ledvina, A. R.; Rose, C. M.; McAlister, G. C.; Syka, J. E. P.; Westphall, M. S.; Griep-Raming, J.; Schwartz, J. C.; Coon, J. J. *J. Am. Soc. Mass Spectrom.* **2013**, *24*, 1623–1633.
- (40) Bourgoin-Voillard, S.; Leymarie, N.; Costello, C. E. *Proteomics* **2014**, *14*, 1174–1184.
- (41) Cannon, J. R.; Holden, D. D.; Brodbelt, J. S. *Anal. Chem.* **2014**, *86*, 10970–10977.
- (42) Brunner, A. M.; Lossel, P.; Liu, F.; Huguet, R.; Mullen, C.; Yamashita, M.; Zabrouskov, V.; Makarov, A.; Altelaar, A. F. M.; Heck, A. J. R. *Anal. Chem.* **2015**, *87*, 4152–4158.
- (43) Rose, C. M.; Russell, J. D.; Ledvina, A. R.; McAlister, G. C.; Westphall, M. S.; Griep-Raming, J.; Schwartz, J. C.; Coon, J. J.; Syka, J. E. P. *J. Am. Soc. Mass Spectrom.* **2013**, *24*, 816–827.
- (44) Michalski, A.; Damoc, E.; Lange, O.; Denisov, E.; Nolting, D.; Müller, M.; Viner, R.; Schwartz, J.; Remes, P.; Belford, M.; Dunyach, J.-J.; Cox, J.; Horning, S.; Mann, M.; Makarov, A. *Mol. Cell. Proteomics* **2012**, *11*, O111.013698.
- (45) Chambers, M. C.; Maclean, B.; Burke, R.; Amodei, D.; Ruderman, D. L.; Neumann, S.; Gatto, L.; Fischer, B.; Pratt, B.; Egertson, J.; Hoff, K.; Kessner, D.; Tasman, N.; Shulman, N.; Frewen, B.; Baker, T. A.; Brusniak, M.-Y.; Paulse, C.; Creasy, D.; Flashner, L.; Kani, K.; Moulding, C.; Seymour, S. L.; Nuwaysir, L. M.; Lefebvre, B.; Kuhlmann, F.; Roark, J.; Rainer, P.; Detlev, S.; Hemenway, T.; Huhmer, A.; Langridge, J.; Connolly, B.; Chadick, T.; Holly, K.; Eckels, J.; Deutsch, E. W.; Moritz, R. L.; Katz, J. E.; Agus, D. B.; MacCoss, M.; Tabb, D. L.; Mallick, P. *Nat. Biotechnol.* **2012**, *30*, 918–920.
- (46) Liu, X.; Inbar, Y.; Dorresteijn, P. C.; Wynne, C.; Edwards, N.; Souda, P.; Whitelegge, J. P.; Bafna, V.; Pevzner, P. A. *Mol. Cell. Proteomics* **2010**, *9*, 2772–2782.
- (47) Fellers, R. T.; Greer, J. B.; Early, B. P.; Yu, X.; LeDuc, R. D.; Kelleher, N. L.; Thomas, P. M. *Proteomics* **2014**, *11*, 649–51.
- (48) Wood, T. D.; Chorush, R. A.; Wampler, F. M.; Little, D. P.; O'Connor, P. B.; McLafferty, F. W. *Proc. Natl. Acad. Sci. U.S.A.* **1995**, *92*, 2451–2454.
- (49) Fabris, D.; Kelly, M.; Murphy, C.; Wu, Z.; Fenselau, C. *J. Am. Soc. Mass Spectrom.* **1993**, *4*, 652–661.
- (50) Reid, G. E.; Wu, J.; Chrisman, P. A.; Wells, J. M.; McLuckey, S. A. *Anal. Chem.* **2001**, *73*, 3274–3281.
- (51) Stephenson, J. L.; McLuckey, S. A. *Anal. Chem.* **1998**, *70*, 3533–3544.
- (52) Coon, J. J.; Ueberheide, B.; Syka, J. E. P.; Dryhurst, D. D.; Ausio, J.; Shabanowitz, J.; Hunt, D. F. *Proc. Natl. Acad. Sci. U.S.A.* **2005**, *102*, 9463–9468.
- (53) Ahlf, D. R.; Compton, P. D.; Tran, J. C.; Early, B. P.; Thomas, P. M.; Kelleher, N. L. *J. Proteome Res.* **2012**, *11*, 4308–4314.
- (54) Meier, S. M.; Tsybin, Y. O.; Dyson, P. J.; Keppler, B. K.; Hartinger, C. G. *Anal. Bioanal. Chem.* **2012**, *402*, 2655–2662.
- (55) Durbin, K. R.; Fellers, R. T.; Ntai, I.; Kelleher, N. L.; Compton, P. D. *Anal. Chem.* **2014**, *86*, 1485–1492.
- (56) Tran, J. C.; Zamdborg, L.; Ahlf, D. R.; Lee, J. E.; Catherman, A. D.; Durbin, K. R.; Tipton, J. D.; Vellaichamy, A.; Kellie, J. F.; Li, M.; Wu, C.; Sweet, S. M. M.; Early, B. P.; Siuti, N.; LeDuc, R. D.; Compton, P. D.; Thomas, P. M.; Kelleher, N. L. *Nature* **2011**, *480*, 254–258.
- (57) Cannon, J. R.; Cammarata, M. B.; Robotham, S. A.; Cotham, V. C.; Shaw, J. B.; Fellers, R. T.; Early, B. P.; Thomas, P. M.; Kelleher, N. L.; Brodbelt, J. S. *Anal. Chem.* **2014**, *86*, 2185–2192.
- (58) Zhao, Y.; Riley, N. M.; Sun, L.; Hebert, A. S.; Yan, X.; Westphall, M. S.; Rush, M. J. P.; Zhu, G.; Champion, M. M.; Medie, F. M.; Champion, P. A. D.; Coon, J. J.; Dovichi, N. J. *Anal. Chem.* **2015**, *87*, 5422–5429.